
Article:
Gonzalez-Buelga, A., Wagg, D.J. and Neild, S.A. (2007) Parametric variation of a coupled pendulum-oscillator system using real-time dynamic substructuring. Structural Control and Health Monitoring, 14 (7). 991 - 1012.

https://doi.org/10.1002/stc.189

Parametric variation of a coupled pendulum-oscillator system using real-time dynamic substructuring

A. Gonzalez-Buelga, D.J. Wagg*and S.A. Neild.

Department of Mechanical Engineering, University of Bristol, Queen's Building, University Walk, Bristol, BS8 1TR, UK.

SUMMARY

In this paper we present results from real-time dynamic substructuring tests used to model the dynamics of a coupled pendulum-oscillator system. The substructuring technique is particularly suitable for systems where the nonlinear and linear parts of the system can be separated. The nonlinear part is built full size and tested physically (the substructure) while the linear part is simulated numerically. Then, in order to replicate the dynamics of the complete system the substructure and the numerical model must be coupled in real-time. In this study we demonstrate how real-time dynamic substructure testing can be used to model systems with strongly nonlinear behavior using parametric variation. We show that the substructuring results give good qualitative and quantitative agreement with purely numerical simulations of the complete system for a range of parameters values. This includes single parameter bifurcation diagrams, some of which cannot be obtained from a full physical experiment. We also briefly discuss the effects of delay and noise on the stability of the substructured system, and how these effects can be mitigated.

*Correspondence to: David.Wagg@bristol.ac.uk, Tel: +44 (117) 9289736, Fax : +44 (117) 929 4423

KEY WORDS: Real-time, Substructuring, Bifurcation, Stability, Accuracy

1. Introduction

In this paper we consider using real time dynamic substructuring to model the dynamics of a well known nonlinear dynamic system. The system chosen is a pendulum coupled to a mass-spring-damper system, which has well known autoparametric resonance behavior [1, 2]. This system, and related mathematical representations, have been studied in depth — see for example [1–5] and references therein. A range of experimental studies of this type of system have also been carried out [6–9]. In addition, this system also has strong relevance to cable-stayed bridge structures, where autoparametric resonances are a significant effect [10, 11].

The connection with structural dynamics is relevant to the work presented in this paper, because it was work in this field that originally motivated the development of dynamic substructure testing. Traditional scaled experimental testing techniques in structural dynamics — such as shaking table testing — have severe limitations when elements of the structure exhibit nonlinear behavior [12]. Engineers have partially overcome this by testing (parts of) full scale structures using delayed time scales, known as pseudodynamic testing (see for example [13–20]). More recently, considerable efforts have been made to develop methods for testing both at large scale and in real time — real time substructuring testing and effective force testing [21–24].

The concept underlying these methods is that only the nonlinear component of interest is tested experimentally, while the remaining part of the structure is computed numerically. In simple systems — such as the one studied in this paper — we can map the linear and

nonlinear parts directly onto the numerical and experimental division. So the pendulum is the nonlinear experimental substructure, and the mass-spring-damper is computed numerically. In structural dynamics testing, this approach allows the single nonlinear element of interest to be tested experimentally, often at full scale. It also allows parameters in the computer model to be varied to undertake parametric testing.

The interface between the nonlinear component and the numerical model is provided by a set of *transfer systems*, which are typically electric or hydraulic actuators. These actuators apply displacements to the nonlinear component via a control system which is designed so that the transfer system follows the appropriate output from the numerical model [22]. Simultaneously, the force required to impose these displacements is measured and fed back into the numerical model to give a two way coupling. The transfer system introduces undesirable dynamics into the system — primarily a phase delay. For accurate results these dynamics, which may (for certain systems) be approximated as a fixed delay, must be compensated for. A variety of compensation mechanisms have been proposed to achieve this [25–28] — we note that related delay compensation techniques have been developed in relation to active control systems for structural control [29–32].

Bifurcation diagrams can normally be generated from a full numerical model of a particular system [33]. However, if the system contains a nonlinear element which cannot be modelled accurately then experimental bifurcation diagrams are the only potential source of information. Unfortunately, designing full scale experiments so that step by step parametric variation can be achieved is non-trivial. Substructuring offers the possibility of experimentally testing the nonlinear element in combination with the appropriate numerical model(s). This has the potential to create hybrid bifurcation diagrams using parameter variation of the numerical

model parameters — which are far easier to vary than experimental parameters.

The purpose of this study is to demonstrate how real time dynamic substructure testing can be used to model systems with strongly nonlinear behavior while parameters are varied to produce bifurcation diagrams [33]. This validation is presented in the later part of this paper where we will assess how well the substructured system compares with a purely numerical simulation of the coupled system. To allow validation of this technique a relatively well known system has been chosen for the study — the coupled pendulum-oscillator system. This system also has the additional benefits of: (i) it can be divided into linear and nonlinear subsystems, (ii) purely numerical solutions can easily be computed to compare with the substructuring test results, (iii) the system has a modelling link to cable-stay bridges, which is an active area of research for substructure testing [34].

Previous experimental studies of autoparametric systems [6–9] have focused on building a complete physical experiment, which can then be compared with analytical and numerical models. Dynamic substructure (also know as hybrid numerical-experimental) testing offers a powerful new versatility — an infinite number of different emulated systems can be tested and studied by varying parameters in the numerical part of the substructuring model. We will show examples of bifurcation diagrams, some of which could not be obtained from full physical experiments.

In the first part of the paper we will discuss the effect of actuator delay and noise. Recent work has shown that even for simple linear substructure elements, the effect of the actuator delay can produce complex dynamics, which can be modelled using delay differential equations (DDE's) [35]. Using a similar approach for the pendulum-mass-spring-damper system leads to neutral differential equations modelling the system [36]. This study demonstrated how the

experimental pendulum mount has a significant effect on the stability boundaries of the system. We show how these effects can be taken into account using phase margin techniques.

We also briefly discuss how the effects of delay and noise can be mitigated using polynomial delay compensation filtering techniques. These combined effects have an influence on accuracy, and in the final part of the paper we discuss how some quantitative measures of how accuracy may be obtained.

2. Description of the system

2.1. Equations of motion

The complete (sometimes referred to as emulated) system that we wish to model is shown schematically in Fig. 1. This system consists of a pendulum mounted with it's pivot point in the center of the mass, M, belonging to the mass-spring-damper. The pendulum mass, m is assumed to act at a single point, a distance l from the pivot point. The equations of motion for the complete system are given by

$$(M+m)\ddot{y} + C\dot{y} + Ky + ml[\ddot{\theta}\sin\theta + \dot{\theta}^2\cos\theta] = F_e, \tag{1}$$

$$ml^2\ddot{\theta} + b_1\mathrm{sgn}(\dot{\theta}) + b_2\dot{\theta} + b_3(\dot{\theta})^2\mathrm{sgn}(\dot{\theta}) + mgl\sin(\theta) + ml\ddot{y}\sin(\theta) = 0, \tag{2}$$

where y is the displacement of the mass M, θ is the angular displacement of the pendulum which has mass m and length l, C and K are the damping and stiffness of the mass-spring-damper respectively, b_1, b_2 and b_3 represent the Coulomb, viscous and air resistance damping of the pendulum respectively, g is acceleration due to gravity, F_e is the external exciting force and $\mathrm{sgn}(\cdot)$ is the signum function.

The natural frequency of the pendulum is $\omega_p = \sqrt{g/l}$, the natural frequency of the complete

system when $\theta = \dot{\theta} = 0$, $\omega_{nm} = \sqrt{K/(M+m)}$ and the frequency of the external driving force is $\omega_e = 2\pi f_e$, where $F_e = \alpha \sin(2\pi f_e t)$ and α is the forcing amplitude in Newtons and f_e is the forcing frequency in cycles per second.. The natural frequencies of the system are ω_p and ω_{nm}. The mass-spring-damper acts as a parametric excitation of the pendulum, and for particular sets of parameter values, the pendulum affects the mass-spring-damper by either adding energy to or absorbing energy from it [1, 37].

The inclusion of three damping terms for the pendulum (corresponding to terms with the coefficients b_1, b_2 and b_3) is to obtain a high degree of correlation between experimental and numerical results. Results from a set of free swinging pendulum tests are shown in Fig. 2. The coefficients b_1, b_2 and b_3 have been selected (see appendix) to give the best fit damping model across a range of both large and small θ values. The result is a maximum error of 2 % or less across the angle range tested.

In the following discussion, y and θ will represent the complete (or emulated) system coordinates. The substructuring model coordinates are denoted by, y^*, which represents the numerical model displacement; x is the experimentally measured pivot motion and θ_x is the experimentally measured angle.

2.2. The real time dynamic substructuring test system

The dynamics of the emulated system shown in Fig. 1 will be studied using real time dynamic substructuring [21]. To achieve this the system is divided into two subsystems. The pendulum is taken to be the physical substructure and the mass-spring-damper is the numerical model. The pendulum pivot point represents the interface between the physical and numerical subsystems.

A real-time substructuring strategy consists of the following steps. The numerical model

is used to calculate the displacement at the interface (pivot) due to some external excitation force, F_e. This displacement is applied to the physical substructure in real-time using a electro-mechanical actuator (the transfer system). The force acting on the physical substructure, F_s is measured via a load cell and fed back into the numerical model. The feedback force acting on the numerical model, $F = F_e - F_s$, is used to calculate the displacement at the interface for the next time step. This process is then repeated until the end of the test.

During the preliminary testing it was found that the platform on which the pendulum pivot is mounted had a significant effect of the substructuring test results. The platform is a mass which has two linear bearings which allow it to move along two parallel rods which can be seen in figure 4. In fact the linear bearing have quite a significant damping effect, estimated to be approximately 10kg/s (Table IV). As the platform is free to move on bearings it effectively has zero stiffness. Therefore, to accurately capture this behavior the mass M is split into two components M_1 and M_2, such that $M = M_1 + M_2$. Now the numerical mass component is M_1 and mass M_2 represents the physical mass of the mounting platform. A similar effect occurs with the viscous damping parameter C, so this too is divided such that $C = C_1 + C_2$, where C_2 corresponds to the physical damping in the mounting platform. A schematic representation of the complete substructuring testing process is shown in Fig. 3.

Including the mounting platform effects, the dynamics of the numerical model as shown in Fig. 3 can be written as

$$M_1\ddot{y}^* + C_1\dot{y}^* + Ky^* = F, \tag{3}$$

where $F = F_e - F_s$. The substructuring force, F_s, can be expressed as a combination of the testing platform and pendulum dynamics, such that

$$F_s = (M_2 + m)\ddot{x} + C_2\dot{x} + ml[\ddot{\theta_x}\sin\theta_x + \dot{\theta_x}^2\cos\theta_x]. \tag{4}$$

where $\ddot{x}$ is the actual acceleration acting on the pivot point and θ_x, $\dot{\theta}_x$ and $\ddot{\theta}_x$ are the measured angle, angular velocity and angular acceleration of the pendulum respectively. When considering the the semi-trivial solution $\theta = \dot{\theta} = 0$, equation (4) simplifies to

$$F_s = (M_2 + m)\ddot{x} + C_2\dot{x}. \tag{5}$$

Physically this corresponds to the case when the pendulum is not moving while the pivot point is subject to an oscillatory motion. Fig. 4 shows a photograph of the experimental pendulum subsystem, actuator and measurement instrumentation. Additional details of the experimental implementation and calibration are given in the appendix.

2.3. Substructuring controller

Under exact matching conditions, the experimentally measured variables, x, and θ_x, would exactly match the emulated variables, y, and, θ, such that $y = y^* = x$ and $\theta = \theta_x$. Such perfect matching cannot be achieved in practice. Instead the objective of the controller is to achieve as high a level of synchronization between y^* and x as possible. Note that we have no direct control over θ_x — in most cases as $y^* \to x$ then $y^* \to y$ and $\theta_x \to \theta$. Exceptions to this are discussed in section 3.

This control problem is typically divided into two parts. First is the basic tracking control, which in this experiment is undertaken by the proprietary proportional controller. We define the transfer system as the actuator and proportional controller combined. The second control task is to use a delay compensation technique, to remove the delay introduced by the transfer system. This technique will be described in detail in section 2.5. This control approach can be considered as a combination of an inner loop controller, which deals with the basic tracking, and an outer loop controller which provides the delay compensation.

2.4. Stability of the real-time dynamic substructuring system

In order to be able to perform successful substructuring tests the coupled real-time substructuring algorithm must remain stable throughout the test. The numerical model, which in this case is a mass-spring-damper, can become unstable due to delays in the transfer system which introduce a negative damping effect [22, 25]. For mass-spring-damper systems this instability has been modelled using delay differential equations [35], where the stability boundary corresponds to a locus of Hopf bifurcations corresponding to zero effective damping in the system [38].

Noise encountered in the experimental system is another effect known to reduce the stability of the system. In fact the problems of delay and noise are strongly related. For example the usual way to reduce delay is to use a forward prediction technique [22, 25, 28] and this in turn can produce a noise amplification effect. If filtering is used to reduce the noise the signal delay will be increased since filters always cause a change in phase. In other words trying to solve one of the problems often has a detrimental effect on the other. The robustness of lightly damped substucturing systems has been considered by [39], where the authors demonstrate how increased robustness can be obtained at the expense of simulation accuracy.

The effect of transfer system delay has been studied by many authors (see for example [25, 26, 35] and references therein). These effects have been considered in detail in a study by [36] for the pendulum-oscillator system considered here. It is worth noting that the effects of damping and inertia in the experimental pendulum mount are significant. Using the same approach as in [36], we model the actuator dynamics as a fixed delay τ, such that

$x(t) = y^*(t-\tau)$. Then by combining equations 3 and 5 we obtain

$$M_1\ddot{y^*} + C_1\dot{y^*} + Ky^* + m_s\ddot{y}^*(t-\tau) + C_2\dot{y}^*(t-\tau) = F_e, \tag{6}$$

where $m_s = M_2 + m$. From this expression the characteristic equation (or complementary function) of the system is found by substituting $y^* = \hat{A}e^{-i\omega t}$ so that

$$-\omega^2\left[M_1 + m_s\cos(\omega\tau)\right] + i\omega[C_1 + m_s\omega\sin(\omega\tau) + C_2\cos(\omega\tau)] + [K + C_2\omega\sin(\omega\tau)] = 0. \tag{7}$$

Equation (7) indicates how actuator delay can potentially cause changes in the effective values of mass, damping and stiffness. However, this case is not easily solved using the DDE analysis discussed by [36]. Instead, we present a more direct approach to studying the stability of the numerical model using Bode diagrams and the concept of phase margin [40].

To do this the dynamics of the numerical model displacement are written using Laplace transform as:

$$Y^*(s) = \frac{N_m(s)F_e(s)}{1 + F_s(s)N_m(s)T(s)}, \tag{8}$$

where $F_s(s) = m_s s^2 + C_2 s$, $N_m(s) = \dfrac{1}{M_1 s^2 + C_1 s + K}$, $T(s) = e^{-s\tau}$ (representing the delay due to the transfer system) and s is the Laplace variable.

The transfer function between input $F_e(s)$ and output $Y^*(s)$ can now be studied as a typical closed loop system. The stability of the system can be examined via the closed-loop-characteristic-equation (CLCE) given by

$$1 + F_s(s)N_m(s)T(s) = 0 \tag{9}$$

which corresponds to the complementary function given by equation 7. The phase margin for a CLCE gives a measure of the amount of phase shift necessary to make the closed loop system unstable – i.e. the Nyquist contour just crosses the -1 point. By plotting the Bode diagram of

$F_s(s)N_m(s)$ we can estimate the phase margin by measuring the difference between the phase curve and -180 degrees at the point corresponding to the frequency that gives 0dB gain. The phase margin relates directly to the maximum allowable delay (via $T(s)$) before the system becomes unstable. An example is shown in Fig. 5, from which we see that, in this case, the maximum phase delay before stability loss is approximately 0.223 seconds. Using this approach for a particular set of parameter values the phase margin can be calculated and from this the maximum delay and its associated instability frequency can be found using the Bode diagram.

As an illustration of this stability analysis, we show stability charts computed for the pendulum-oscillator system showing the maximum phase delays at which the system goes unstable. This example is shown in Fig. 6 where we demonstrate the effects on the stability boundary as the parameters m_s is varied for two different C_2 cases. The solid line in Fig. 6 corresponds to the stability chart calculated for the case when $C_2 = 0$ with $\omega_n = 10$rad/s and $\zeta = 0.05$. The theoretical stability boundary which occurs when $C_2/C_1 = 1$ is plotted as a dashed line. In Fig. 7 we show a comparison between these two cases and experimental results from the substructuring tests, where $C_2/C_1 = 1$. This shows that a very close agreement exists between the experimental results and the case when $C_2/C_1 = 1$ — indicating why the effect of damping feedback, C_2 is significant. The experimental points were obtained by adding additional masses to the end of the pendulum to change the mass ratio $p = m_s/M_1$. The stability boundary points were then located by artificially increasing the delay (by holding the signal sent to the actuator during the experiment) until the instability frequency appears. As expected for each mass configuration there is a corresponding change in maximum delay and instability frequency.

2.5. Delay compensation

It is clear that delays present in the experimental system have a significant effect on the stability of the coupled substructuring system. The effect of delay on accuracy will be discussed in section 4. One way to try to eliminate (or at least reduce) the delay is to forward predict the relevant signals, [22,25,28]. This is achieved by first estimating the delay, τ, present in the system. Then instead of sending the target, $y^*(t)$ signal to the transfer system, an estimation of $y^*(t+\tau)$ is sent. The delay present in the transfer system can be measured in real time by using synchronization subspace plots [28] which are described in subsection 4. If the experimental substructure is linear and there is no significant noise, the desired displacement, can be achieved by using a polynomial forward prediction technique — typically polynomials of fourth order or more have been shown to give effective results [25,35].

In the presence of nonlinearities or noise, as in this case, high order polynomial fitting is not desirable due to the tendency for these methods to amplify noise. For the substructuring tests in this paper a first order polynomial technique, following the approach described by [28], has been found to give an acceptable trade off between noise amplification and accuracy. Good results have been achieved by recording 5 points which are fitted to a straight line. This method is simple and highly effective provided that the time steps are small enough — in the experimental results presented in this work the time step was 1ms and the actuator delay approximately 18ms.

2.6. Dealing with unmodeled dynamics and noise

The primary source of noise occurs when measuring the force feedback signal, F_s, from the physical substructure. In the experimental system considered here the noise is primarily caused

by a combination of the following two effects. First there are high frequency mechanical vibrations induced by the actuator servo motor. This makes the experimental testing platform vibrate in odd harmonics of the actuator target signal. Secondly electrical noise is present in the experimental testing area. Despite isolating the measurement transducers there is still a significant level of electrical noise in the force transducer signal. The fact that the system is part inertial and that acceleration is highly sensitive to noise only increases these effects. In most of the substructuring testing cases studied here the system can deal with the noise present in this signal. In fact the mass-spring-damper (numerical model) acts like a filter of its input force and depending on the parameter values damps out a proportion of the undesired frequencies.

Introducing additional filtering will also introduce additional delay. So where possible, additional filtering of signals during real time testing should generally be avoided. However for a range of numerical model parameters values the numerical model can lose stability due to the unmodeled dynamics present in the system. The system is particularly susceptible to this when the phase margin (computed via equation 8) is small and the feedback force F_s, is significantly larger than the external force F_e. This type of instability (which is essentially due to insufficient robustness) manifests itself as the sudden appearance of high frequencies in the actuator displacement, x. Figure 7 (a) shows an experimental recorded example of instability due to unmodeled dynamics, where the maximum permissible phase delay is only 9ms.

In this study, we are primarily interested in a small range of frequencies, where the parametric resonances occur and the nonlinear and chaotic pendulum behavior appears. As a result a narrow band filter can be designed, with cut-off frequencies dependent on each particular case to mitigate the effect of noise in the feedback force signal. This filter is

characterized by a flat unity magnitude response in the passband, the change in phase that the filter causes to the primitive signal is treated as delay. An example is shown in Fig. 7 (b). In this example at 2.2 Hz, the difference in phase caused by the filter at the given frequency is -0.2185rad which is equivalent to a delay of τ=0.0158s. To compensate for the delay induced by the filter, the signal is predicted forward before being sent to the numerical model.

3. Substructuring test results

We start this section by considering substructuring tests without parameter variation. Previous experimental studies of autoparametric systems [6–9] have focused on building a complete physical experiment, which can then be compared with analytical and numerical models. Thus the first step in this process is to show that substructure models can capture the full range of dynamical behavior typically encountered by our example system. Beyond this, we will demonstrate in this section how the methods can be extended to include parametric variations, leading to bifurcation diagrams. In fact, substructuring offers a powerful new versatility — an infinite number of different emulated systems can be tested and studied by varying parameters in the numerical part of the substructure model. We will demonstrate this with results from the pendulum-oscillator system.

3.1. Modelling typical dynamics of the pendulum oscillator system

In this subsection we will briefly demonstrate that the substructuring system can capture a range of dynamics typical of the pendulum-mass-spring-damper system, by choosing some specific examples. The first case we consider occurs when the mass-spring-damper (or primary system) is in 2:1 resonance with the pendulum (or secondary system), such that $\omega_e = \omega_{nm} =$

$2\omega_p$. This example is well known and has been studied in detail, comprehensive summaries can be found in [1,2]. At this 2:1 ratio of frequencies it is possible for certain parameter values that energy from the mass-spring-damper is transferred to the pendulum, which acts as a vibration absorber — sometimes called the strongly quenched solution. Two coexisting solutions exist with maximum amplitudes given by

$$y_{1max} = \frac{a}{\sqrt{(\omega_{nm}^2 - \omega_e^2)^2 + (\kappa\omega_e)^2}} \quad \text{and} \quad y_{2max} = 2l\sqrt{\left(\frac{\omega_p^2}{\omega_e^2} - \frac{1}{4}\right)^2}. \tag{10}$$

where $\kappa = C(M+m)$, and $a = \alpha/(M+m)$, see [2] for further details.

This energy transfer behavior was simulated using the substructuring testing rig and the results are shown in Fig. 8. . In this example the parameters are $\alpha = 2$N and $f_e = 2.25$Hz (where $\omega_e = 2\pi f_e$), $M = M_1 + M_2 = 10.9$kg, $C = C_1 + C_2 = 20$kg/s, and $K = 1910$N/m. For these parameters, the theoretical maximum amplitude, $y_{1max} = 0.0041$m, is in close agreement with the corresponding substructuring test value of maximum amplitude measured experimentally as $x_{1max} = 0.004$m. The theoretical maximum amplitude for $y_{2max} = 4.2 \times 10^{-4}$m is also in close agreement with the corresponding substructuring test value of maximum amplitude measured experimentally as $x_2 = 5 \times 10^{-4}$m. This example shows a high level of agreement between the substructuring results and the theoretically computed values.

In Fig. 9 we show two further examples of typical steady-state motions of the pendulum-oscillator system. In this figure the substructuring test results are shown as a solid line. This can be compared with a fully numerical simulation of the complete system, which is shown as a dashed line The full numerical simulation was computed by simulating Eq.s (1) and (2) in

first order form with $z_1 = y$, $z_2 = \dot{y}$, $z_3 = \theta$, $z_4 = \dot{\theta}$, such that

$$\begin{Bmatrix} \dot{z_1} \\ \dot{z_2} \\ \dot{z_3} \\ \dot{z_4} \end{Bmatrix} = \begin{Bmatrix} z_2 \\ \frac{1}{M + m\cos^2(z_3)} \left[F_e - Cz_2 - Kz_1 + mg\sin^2(z_3) - mlz_4^2\cos(z_3) + \frac{\sin(z_3)}{l} f_d \right] \\ z_4 \\ \frac{-\sin(z_3)/l}{M + m\cos^2(z_3)} \left[F_e - Cz_2 - Kz_1 + (M+m)g - mlz_4^2\cos(z_3) + \frac{\sin(z_3)}{l} f_d \right] - \frac{f_d}{ml^2} \end{Bmatrix}. \tag{11}$$

where $f_d = b_1\mathrm{sgn}(z_4) + b_2 z_4 + b_3 z_4^2\mathrm{sgn}(z_4)$, represents the damping in the pendulum. This state space model is solved numerically using a 4th order Runge-Kutta integration method. The time step used was 1ms, identical to the sampling time used in the substructuring tests. For each fixed step the signum function was evaluated to give the damping force, f_d. Fig 10 shows two different orbits with a $\omega_n/\omega_p = 1.8687$ frequency ratio between the pendulum and mass-spring-damper and a $\hat{\omega} = \omega_e/2\omega_p = 0.9757$ frequency ratio between the pendulum and the external exciting force. Fig. 9 (a) shows a periodic orbit which exists when the external force amplitude is $\alpha = 5N$. In this case very close agreement exists between the substructuring results and the full numerical simulations. In Fig. 9 (b) a comparison between a substructured chaotic orbit and it's numerically computed version is shown, in this case the external force amplitude is $\alpha = 12N$. Due to sensitivity of initial conditions it is not possible to achieve a high level of quantitative agreement when comparing the chaotic time series — although this is also the case for full physical experiments. Qualitatively we observe that both substructured and fully numerical simulations exhibit chaotic motion under the action of the same external excitation force. The divergence of the trajectories is due primarily to the noise present and difficulties in setting the initial conditions in the experiment to match the full numerical simulation.

3.2. Parametric variation

We now consider comparing the substructuring test results to full numerical simulations for ranges of system parameter values. The first example we consider is the point at which semi-trivial solution has a Hopf bifurcation. These points form a boundary in a two dimensional parameter space (forcing amplitude and forcing frequency) which defines where the semi-trivial solution ceases to exist — we will call it the Hopf bifurcation boundary. In fact, for the case where ω_e is close to $2\omega_p$ and $b_1 = b_3 = 0$ an analytical relationship for the Hopf bifurcation boundary of the semi-trivial solution can be developed (see [2] and references therein). For the parameters in our example this can be expressed as

$$\alpha^2 \leq l^2\omega_e^4(M+m)^2\left[\left(\frac{\kappa}{\omega_e}\right)^2+\sigma^2\right]\left[\left(\frac{\kappa_p}{\omega_e}\right)^2+\sigma_p^2\right], \tag{12}$$

where $\kappa_p = b_2/(ml^2)$, $\sigma = [(\omega_{nm}/\omega_e)^2 - 1]$ and $\sigma_p = 2[(\omega_p/\omega_e)^2 - 1/4]$.

From the substructuring tests the Hopf bifurcation boundary was plotted in $(\alpha, \hat{\omega})$ parameter space, where $\hat{\omega} = \omega_e/(2\omega_p)$ and α is the magnitude of the external exciting force. This was compared with the Hopf bifurcation boundary given by Eq. (12), and the results are shown in Fig. 10 (a). In these substructure tests for each value of $\hat{\omega}$ the amplitude of the external force is increased until the pendulum starts moving — indicating that the semitrivial solution has reached the Hopf bifurcation boundary. Fig. 10 (a) shows that there is very good agreement between the substructuring experimental results and the analytical boundary given by Eq. (12) for the selected parameter range. In addition, the position of the periodic orbit (PO) and chaotic example (CO) shown in Fig. 9 are marked on Fig. 10 (a).

The structure of the substructuring testing algorithm means that it is straight forward to vary parameters in the numerical subsystem. As a result we can consider how the Hopf bifurcation boundary in $(\alpha, \hat{\omega})$ space changes as an additional parameter is varied. An example

of this is shown in Fig. 10 (b), where four different values of M have been selected, and the Hopf bifurcation boundary of the semi-trivial solution computed for each case. For clarity, only the substructuring experimental results are shown in Fig. 10 (b), but in each case a similar level of agreement with the analytical solution as that shown in Fig. 10 (a) is found.

The final example we show in this section are single parameter bifurcation diagrams. For the substructuring tests these are computed by allowing 100 transient periods to decay before recording maximum amplitudes for 20 steady state periods of motion for each parameter step. The results from these tests are shown in Fig. 11. Fig. 11 (a1) shows a single parameter bifurcation diagram for the system as the forcing amplitude is varied through the range $0 \leq \alpha \leq 45$N. This figure follows the line of cross-section A shown on Fig. 10 (a). For $\alpha < 15$N the semi-trivial solution is stable, and $\theta_{max} = 0$rad. At $\alpha \approx 16$N the semi-trivial crosses the Hopf bifurcation boundary, and there is a small region of quasi-periodic motion before a period-2 motion becomes established. The periodic motion lasts until $\alpha \approx 39$N before a jump to chaos occurs. Fig. 11 (a2) shows the parameter bifurcation diagram obtained from a full numerical simulation. There is a close agreement between the substructured and full numerical simulations across the parameter range considered.

So far all the results we have shown could have been obtained by constructing a complete physical experiment of the system, and varying the forcing amplitude and frequency. To obtain the results shown in Fig. 10 (b) from a complete experimental system, the mass M would need to be physically adjusted for each set of tests — impractical but not impossible. In this final example mass is varied through a parameter range – a simulation which could not practically be obtained from a full physical experiment, but can be obtained using a substructured model (and, of course, also by a full numerical model). This is a single parameter bifurcation diagram

for $0 \leq M \leq 13$kg and the results are shown in Fig. 11 (b1). Again we see a progression from the stable semi-trivial solution through quasi-periodic and periodic motion to a window of chaotic motion. Fig. 11 (b2) shows the corresponding parameter bifurcation diagram obtained when from fully numerical simulation. As with the previous case, there is a close agreement between the substructured and full numerical simulations across the parameter range considered.

As M is then increased further, periodic motion is encountered before a return to the semi-trivial solution occurs. This example highlights how real time dynamic substructure testing may be exploited to obtain results which cannot be found from a full physical experiment.

4. Accuracy of the real time dynamic substructure test results

Estimating the accuracy (how close our result is to the emulated system values) of substructure testing is currently an active area of research [35, 41]. The most straightforward way of measuring accuracy is comparison with a purely numerical simulation, which we have demonstrated in the previous sections. This can be done recognizing that the numerical simulation will have its own limitations — although the pendulum-oscillator system is such a simple and well known example that we can have a high degree of confidence that the numerical simulations give a good model of the dynamics. For more complex systems, complete simulation is not always possible due to limitations of the relevant mathematical models. In this case other methods for measuring accuracy must be used, and in this section we will describe a method based on synchronization subspace techniques [28,41]. In particular we will assess the accuracy of our experiments by studying the synchronization error [28]. Alternative energy methods have been discussed by [13, 41].

Using the synchronization subspace approach, the synchronization error — target

displacement (calculated through the analytical model) minus the measured displacement — is monitored in order to detect sources of systematic error. Here we consider systematic errors to be those which come from non-random sources. Random errors — such as electrical noise — can usually be mitigated by using averaged measurements. Systematic errors however, can have a serious affect on the accuracy of the experiment. When monitoring experimental error, deviations from broadband random noise can indicate the presence of systematic errors. The synchronization approach is based on the techniques of synchronization subspace as defined by [42] and extended for substructuring by [28].

To carry out the error assessment, a graph consisting of target versus measured displacement is plotted. The *synchronization subspace* is defined as the manifold on which $x = y^*$, which in this case is a straight 45 degree gradient line. If the plotted trajectory lies on the synchronization subspace, this indicates perfect correlation. Deviations from the synchronization subspace indicate poor performance of the control method, and can give an indication of the type of systematic error present [28].

A good level of correlation between target and measured displacements was noted for all the tests performed — an example is shown in Fig. 12 (a). Here all the experimental points are very close to the 45 degree gradient indicating *qualitatively* that the accuracy obtained was high. Fig. 12 (b) shows the synchronization error $(y^* - x)$ as a time series, for the periodic and chaotic motions shown in Fig. 9. This information gives a limited quantitative measure of error for each test. In Fig. 12 (c) the power spectral densities of the synchronization error signal have been plotted in order to detect any pattern present in the error signals. For both tests this shows that the predominant frequency in the error signal is similar to the external driving frequency, which can clearly be seen in Fig. 12 (b). The largest source of systematic errors at

the forcing frequency are amplitude and phase errors in the control process and Fig. 12 shows the residual errors after the control and delay compensation methods have been applied. It should be noted that the amplitudes of all the errors shown in Fig. 12 are small relative to the amplitude of displacement of the signals — for example in Fig. 9.

Motion	Maximum synchronization error [m]	Maximum target [m]	ratio [%]
PO	0.0007	0.0181	3.9
CO	0.0016	0.0405	3.9

Table I. Relative synchronization errors

In fact, a way to measure the effect of the synchronization error on the experiment results is by comparing maximum synchronization error with maximum target displacement [41]. The results of this for the two time series shown in Fig 9 are shown in table 1, where the relative error in both cases is below 5 percent. Although this is a quantitative measure, how this level of error propagates into global errors between the emulated and substructuring results depends on the sensitivity of the system to small perturbations. This was clearly the effect shown in Fig. 9, where periodic motion is robust to small perturbations, whereas the chaotic orbit is highly sensitive (see [43] for a recent discussion on error growth in nonlinear models).

5. Conclusions

In this paper we have presented results from a real-time dynamic substructuring model of a pendulum-oscillator system — a system which is known to exhibit a range of nonlinear behavior such as autoparametric resonance. The main purpose of this study was to demonstrate how substructure testing could be used to model systems with strongly nonlinear behavior and

parametric variation. In the substructure model, the experimental test piece was a pendulum, and the mass-spring-damper was modelled numerically. The two parts of the model were coupled together using real time control, and forward prediction techniques.

We have briefly discussed the effects of delay and noise on the stability of the substructuring system. In particular we noted how both the inertia and damping in the experimental pendulum mount had a significant effect on the system stability — which could be estimated using phase margin techniques. The effect of delays in the transfer system were minimized by using a polynomial forward prediction technique. The effect of noise was mitigated using a filtering technique. This was required to increase the system robustness when the phase margin was small, in which case, without filtering the noise would destabilize the system.

Using these techniques the substructuring modelling results were shown to give good qualitative agreement with purely numerical simulations of the complete system. Examples of quenching and the Hopf bifurcation boundary of the semitrivial solution were used to show this comparison. In addition we have shown results for single parameter bifurcation tests. By using the numerical parameters in the substructured system, we showed how examples of bifurcation diagrams can be found which could not be obtained from a full physical experiment. Finally we have discussed how some quantitative measures of accuracy can be assessed from synchronization subspace plots.

Real-time dynamic substructuring is highly significant for structural dynamics testing. In this small scale study of a pendulum-oscillator system we have demonstrated how real-time dynamic substructuring can be used to model parameter variation leading to bifurcation diagrams. We anticipate that this approach can be applied to larger scale structural tests with nonlinear elements where accurate numerical modelling of the entire system is not possible..

Acknowledgments

The authors would like to acknowledge the support of the EPSRC: Alicia Gonzalez-Buelga is supported by EPSRC grant (GR/S49780) and David Wagg via an Advanced Research Fellowship. The authors would also like to thank Alan Champneys, Yuliya Kyrychko and John Hogan for useful discussions regarding this work.

Appendix: Experimental implementation and calibration

To implement the real-time tasks a dSpace DS1104 RD controller board was used. MATLAB/Simulink was used to build the substructuring model shown in Fig. 3. In particular the numerical model of the mass-spring-damper was implemented here, which once downloaded to the dSpace board provides real time computations. The displacement output from the numerical model was computed using a 4th order Runge-Kutta type explicit integration scheme. The dSpace module ControlDesk is used for on line analysis and control. All these elements together provide one integrated tool to manage the real-time substructuring experiments.

The transfer system consists of an electrically driven ball-screw actuator with an in line mounted synchronous servo motor controlled by a servo drive which applies a displacement to the pendulum pivot point in the vertical direction. Figure 4 shows a photograph of the experimental apparatus. The instrumentation used consists of a load cell to measure the force acting at the pendulum pivot, a LVDT displacement transducer connected to the platform to be able to track and control the actuator movement and a digital incremental encoder used to record both angular displacement and angular velocity of the pendulum. Table

III shows the calibration constants for the used sensors. The experimental rig is mounted vertically on a heavy steel frame to limit external vibration. The fixed test rig parameters were measured/estimated and are shown in Table IV. The other system parameters M_1, K and C_1 are set in the numerical model code.

The experimental pendulum damping values were estimated as follows: we select a set of initial values for $b1$, $b2$ and $b3$. As air resistance is known to be small we use an initial value of $b3 = 0$. For small angles Coulomb damping is dominant, so we estimate an initial value for b_2 from a linear fit of the data shown in Fig. 2 (a). For large angles viscous damping is dominant, so we estimate an initial value for b_1 from an exponential of the data shown in Fig. 2 (b). The three initial values are then updated to obtain a best fit over the full angle range using a sensitivity matrix approach [44].

p	0.2250	0.2925	0.4550	0.6175
Experimental	32	34	40	45
Theoretical	31	32	37	44

Table II. Theoretical versus experimental instability frequencies, [rad/s] for the inertial plus viscous damping force feedback case. The p ratio was adjusted experimentally by adding mass to the pendulum in increments of 650g.

	LVDT	Load cell	Encoder
range	150mm	250N	1.26×10^5rad
sensitivity	32.31mV/mm	0.0402V/N	0.0013 rad/pulse

Table III. Measuring devices characteristics

m	l	b_1	b_2	b_3	ω_p	$2f_p$	M_2	C_2
kg	m	kgm^2/s^2	kgm^2/s	kgm^2	rad/s	Hz	kg	kg/s
0.27	0.1955	3.01411×10^{-4}	4.5067×10^{-5}	9.17×10^{-7}	7.0837	2.2548	0.9	10

Table IV. Test rig parameters

REFERENCES

1. M. Cartmell. *Introduction to linear, parametric and nonlinear vibrations*. Chapman and Hall, 1990.
2. A. Tondl, T. Ruijgrok, F. Verhulst, and R. Nabergoj. *Autoparametric Resonance in Mechanical Systems*. Cambridge, 2000.
3. R. Svoboda, A. Tondl, and F. Verhulst. Autoparametric resonance by coupling of linear and non-linear systems. *International Journal of Non-Linear Mechanics*, 29(2):225–232, 1994.
4. S. Fatimah and M. Ruijgrok. Bifurcations in an autoparametric system in 1:1 internal resonance with parametric excitation. *International Journal of Non-Linear Mechanics*, 37:297–308, 2002.
5. W. Q. Zhu and Z. H. Liu. Homoclinic bifurcation and chaos in coupled simple pendulum and harmonic oscillator under bounded noise excitation. *International Journal of Bifurcation and Chaos*, 15(1):233–243, 2005.
6. A. Berlioz, R Dufour, and S.C. Sinha. Bifurcation in a nonlinear autoparametric system using experimental and numerical investigations. *Nonlinear Dynamics*, 23:175–187, 2000.
7. I. Cicek and A. Ertas. Experimental investigation of beam-tip mass and pendulum system under random excitation. *Nonlinear Dynamics*, 16:1059–1072, 2002.
8. O. Cuvalci. The effect of detuning parameters on the absorption region for a coupled system: a numerical and experimental study. *Journal of Sound and Vibration*, 229:837–857, 2000.
9. O. Cuvalci, A. Ertas, S. Ekwaro-Osire, and I. Cicek. Non-linear vibration absorber for a system under sinusoidal and random excitation: Experiments. *Journal of Sound and Vibration*, 249:701–718, 2002.
10. V. Gatulli, M. Lepidi, J.H.G. Macdonald, and C.A. Taylor. One to two global local interaction in a cable-stayed beam observed through analytical, finite element and experimental models. *International Journal of Non-linear Mechanics*, 40:571–588, 2005.
11. J.H.G. Macdonald and C.T. Georgakis. The influence of cable-deck interaction on the seismic response of cable-stayed bridges. In *Proc. 12th Euro. Conf. Earthquake Eng.*, pages 157–164, London, 2002. Elsevier.
12. M.S. Williams and A. Blakeborough. Laboratory testing of structures under dynamic loads: an introductory review. *Phil. Trans. R. Soc. Lond. A*, 359:1651–1669, 2001.
13. P-S. Shing and S. A. Mahin. Cumulative experimental errors in pseudodynamic tests. *Earthquake Engineering and Structural Dynamics*, 15:409–424, 1987.
14. Masayoshi Nakashima, Hiroto Kato, and Eiji Takaoka. Development of real-time pseudo dynamic testing. *Earthquake engineering and structural dynamics*, 21:79–92, 1992.

15. C. Thewalt and M. Roman. Performance parameters for pseudodynamic tests. *Journal of Structural Engineering*, 120(9):2768–2781, 1994.
16. O.S. Bursi and P.B. Shing. Evaluation of some implicit time-stepping algorithms for pseudodynamic tests. *Earthquake Engineering and Structural Dynamics*, 25(4):333–355, 1996.
17. J. Donea, P. Magonette, P. Negro, P. Pegon, A. Pinto, and G. Verzeletti. Pseudodynamic capabilities of the elsa laboratory for earthquake testing of large structures. *Earthquake Spectra*, 12(1):163–180, 1996.
18. G. Magonette. Development and application of large-scale pseudo-dynamic testing techniques. *Philosophical Transactions of the Royal Society A*, 359(1786):1771–1799, 2001.
19. M. Nakashima. Development, potential, and limitations of real-time online (pseudo dynamic) testing. *Philosophical Transactions of the Royal Society A*, 359(1786):1851–1867, 2001.
20. A.V. Pinto, P. Pegon, G. Magonette, and G. Tsionis. Pseudo-dynamic testing of bridges using non-linear substructuring. *Earthquake Engineering and Structural Dynamics*, 33:1125–1146, 2004.
21. A. Blakeborough, M. S. Williams, A. P. Darby, and D. M. Williams. The development of real-time substructure testing. *Philosopical Transactions of the Royal Society of London A*, 359:1869–1891, 2001.
22. A. P. Darby, A. Blakeborough, and M. S. Williams. Improved control algorithm for real-time substructure testing. *Earthquake Engineering and Structural Dynamics*, 30:431–448, 2001.
23. D. J. Wagg and D. P. Stoten. Substructuring of dynamical systems via the adaptive minimal control synthesis algorithm. *Earthquake Engineering and Structural Dynamics*, 30:865–877, 2001.
24. S.A. Neild, D.P. Stoten, D. Drury, and D.J. Wagg. Control issues relating to real-time substructuring experiments using a shaking table. *Earthquake Engineering and Structural Dynamics*, 34:1171–1192, 2005.
25. T. Horiuchi, M. Inoue, T. Konno, and Y. Namita. Real-time hybrid experimental system with actuator delay compensation and its application to a piping system with energy absorber. *Earthquake Engineering and Structural Dynamics*, 28:1121–1141, 1999.
26. A. P. Darby, M. S. Williams, and A. Blakeborough. Stability and delay compensation for real-time substructure testing. *ASCE Journal of Engineering Mechanics*, 128(12):1276–1284, 2002.
27. P.J. Gawthrop, M.I. Wallace, and D.J. Wagg. Bond-graph based substructuring of dynamical systems. *Earthquake Engineering and Structrural Dynamics.*, 34(6):687–703, 2005.
28. M.I. Wallace, D.J. Wagg, and S.A. Neild. An adaptive polynomial based forward prediction algorithm for multi-actuator real-time dynamic substructuring. *Proceedings of the Royal Society of London A. In press.*, 461(2064):3807–3826, 2005.
29. S. McGreevy, T. T. Soong, and A. M. Reinhorn. An experimental study of time delay compensation

in active structural control. In *Proceedings of the 6th International Modal Analysis Conference-IMAC*, volume 1, pages 733–739, 1988.

30. T. T. Soong. *Active Structural Control: Theory and Practice*. Longman, London and Wiley, New York, 1990.
31. A. K. Agrawal and J. N. Yang. Compensation of time-delay for control of civil engineering structures. *Earthquake Engineering & Structural Dynamics*, 29:37–62, 2000.
32. S. Y. Chu, T. T. Soong, and A. M. Reinhorn. *Active, hybrid and semi-active structural control*. John Wiley:Chichester, England., 2005.
33. J. M. T. Thompson and H. B. Stewart. *Nonlinear dynamics and chaos*. John Wiley: Chichester, 2002.
34. A. Gonzalez-Buelga, D. J. Wagg, M. I. Wallace, S. A. Neild, and J. H. G. Macdonald. Testing an autoparametric pendulum using a hybrid numerical experimental method. In *Proceedings of the 1st International Conference on Advances in Experimental Structural Engineering*, volume 1, pages 417–424, 2004.
35. M.I. Wallace, J. Sieber, S.A. Neild, D.J. Wagg, and B. Krauskopf. Stability analysis of real-time dynamic substructuring using delay differential equation models. *International Journal of Earthquake Engineering and Structural Dynamics (Currently available via early view)*, 34(15):1817–1832, 2005.
36. Y. N. Kyrychko, K. B. Blyuss, A. Gonzalez-Buelga, S. J. Hogan, and D.J. Wagg. Real-time dynamic substructuring in a coupled oscillator-pendulum system. Accepted for publication in Proceedings of the Royal Society A., 2005.
37. D. Acheson. *From Calculus to Chaos*. Oxford University Press, 1997.
38. D. E. Gilsinn. Estimating critical hopf bifurcation parameters for a second order delay differential equation with application to machine tool chatter. *Nonlinear Dynamics*, 30:103–154, 2002.
39. P.J. Gawthrop, M.I. Wallace, S.A. Neild, and D.J. Wagg. Robust real-time substructuring techniques for lightly-damped systems. *Journal of Structural Control & Health Monitoring: Available via early view.*, 2006.
40. G. C. Goodwin, S. F. Graebe, and M. E. Salgado. *Control System Design*. Pearson, 2000.
41. G. Mosqueda. *Continuous Hybrid Simulation with Geographically Distributed Substructures*. PhD thesis, University of California, Berkeley, 2003.
42. P. Ashwin, J. Buescu, and I. Stewart. Bubbling of attractors and synchronisation of chaotic oscillators. *Physics Letters A*, 193:126–139, 1994.
43. J. Harlim, M. Oczkowski, J. A. Yorke, E. Kalny, and B. R. Hunt. Convex error growth patterns in a

global weather model. *Physical Review Letters*, 94:228501–1–228501–4, 2005. Art No. 228501.

44. M.I. Friwell and J.E. Mottershead. *Finite Element Updating in Structural Dynamics*. Kluver Academic Publishers, 1999.

Figure captions

- **Figure 1** Schematic representation of the complete pendulum-mass-spring-damper system.
- **Figure 2** Pendulum damping identification from free swinging pendulum tests; (a) Coulomb damping for small angles, estimating b_2; (b) Viscous damping for large angles, estimating b_1; (c) Combined damping contributions b_1, b_2 and b_3 adjusted by using a sensitivity matrix iterative updating method [44], giving the closest match between numerical and experimental data. For clarity, only the envelope (i.e. max/min values) of the numerical simulation is shown in comparison with experimental data..
- **Figure 3** A schematic representation of the real time dynamic substructure testing method for the pendulum-oscillator system.
- **Figure 4** Photograph of the physical substructure tested in the laboratory.
- **Figure 5** Phase margin calculation. The difference in phase between the phase curve and -180 degree line at the point corresponding to the frequency that gives 0dB gain. Parameters values for the example: $M_1 = 20$kg, $C_1 = 20$kg/s, $K = 2000$N/m, $m = 10$kg, $C_2 = 20$kg/s. Phase margins: $\omega_1 = 14.1$rad/s, $\psi_1 = 180$degrees, $\omega_2 = 8.16$rad/s, $\psi_2 = 332.5$degrees. First stability switch $\frac{\psi_2 \pi}{\omega_2 180} = 0.223$s, second stability switch $\frac{\psi_1 \pi}{\omega_1 180} = 0.711$s.
- **Figure 6** Effects of the viscous delayed feedback in the stability chart showing experimental versus theoretical results. The experimental points are compared with the two C_2 cases. Numerical model parameters: $M_1 = 4$kg, $C_1 = 10$kg/s and $K = 3000$N/m, $C_2/C_1 = 1$.
- **Figure 7** Filtering a noisy force signal. Numerical model parameters: $M_1 = 1$kg,

$C_1 = 5$kg/s and $K = 12000$N/m. Maximum delay allowed from the phase margin analysis $\tau_{max} = 0.009$s. (a) The substructuring system becomes unstable due to noise; (b) A narrow filter designed around the frequency range of interest is designed. The filter is characterized by a flat unity magnitude response in the passband and a change in phase that is treated as a delay. This delay will be compensated for by using a prediction forward technique. In the example shown here, for $\omega = 2.2$Hz the additional delay is found to be τ=0.0158s.

- **Figure 8** Real time dynamic substructuring example showing the energy transfer between solutions when $\omega_e \approx \omega_{nm} \approx 2\omega_p$, ST: semitrivial solution, NT: nontrivial solution. Numerical model parameters: $M_1 = 10$kg, $C_1 = 10$kg/s and $K = 1910$N/m. External exciting force $\alpha = 2$N $f_e = 2.25$Hz. Experimentally the transition is instigated by perturbing the pendulum by θ=0.1rad.
- **Figure 9** Real time dynamic substructuring results compared with full numerical simulations. Parameters values: $M = 10.9$kg, $C = 20$kg/s, $K = 1910N$/m; (a) $\alpha = 5$N $f_e = 2.20$Hz, $\hat{\omega} = 0.9757$, Pendulum periodic, shown as PO on figure 9(a); (b) $\alpha = 12$N $f_e = 2.20$Hz, $\hat{\omega} = 0.9757$, Pendulum chaotic, shown as CO on figure 9(a).
- **Figure 10** Semitrivial solution stability in 2-dimensional parameter space α vs $\hat{\omega}$. (a) Real time dynamic substructuring versus analytical results. Grey line: theoretical stability border. Stars: substructuring experimental Hopf bifurcation boundary. Crosses: position of the examples shown in figure 9. Vertical dotted line: cross section A shown in figure 11(a1). Parameters: $M = 10.9$kg, $C = 20$kg/s, $K = 1910$N/m; (b) substructuring experimental results showing the boundary of the semitrivial solution for a range of $5.9 \leq M \leq 20.9$kg. Fixed values $C = 20$kg/s, $K = 1910$N/m.

- **Figure 11** Experimental bifurcation diagrams: θ_{xmax} steady state values (a1) as the amplitude of the external exciting force is varied (a2) full numerical simulation of the bifurcation diagram with a parameter increment of 0.5N. Other parameters in (a1) and (a2): $M = 10.9$kg, $C = 20$kg/s, $K = 1910$N/m, $f_e = 2.5$Hz. (b1) substructuring bifurcation diagram using the numerical model mass M_1 ($M = M_1 + M_2$) as the bifurcation parameter; (b2) full numerical simulation of the bifurcation diagram shown in (b1) using a parameter interval of 0.1kg. Other parameters: $C = 20$kg/s, $K = 1910$N/m, $f_e = 2.5$Hz, $\alpha = 17$N. θ_{xmax} and θ_{max} axis limits $(-\pi, \pi)$.
- **Figure 12** Synchronization error, showing the measured accuracy of the results depicted in Figure 8. (a) Synchronization subspace for the PO example; (b) Synchronization error time series for both PO and CO examples; (c) Synchronization error power spectral density, PO and CO examples: the predominant frequency is the external driving frequency $f_e = 2.20$Hz.

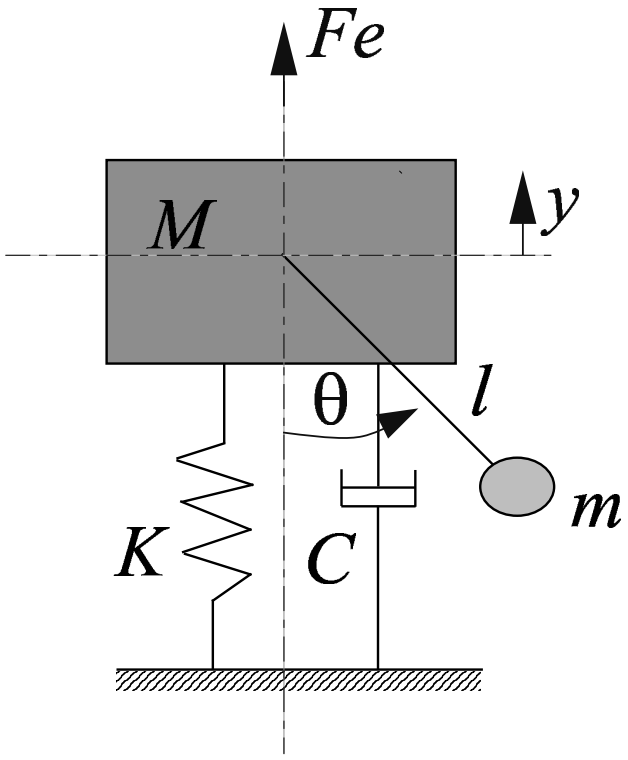

Figure 1.

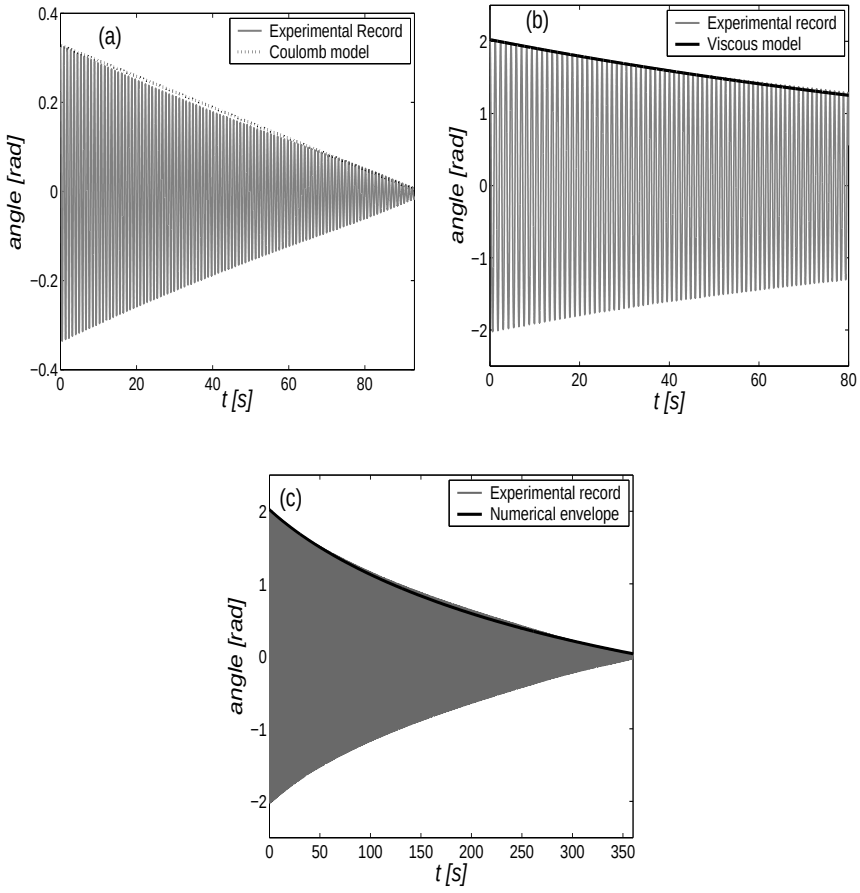

Figure 2.

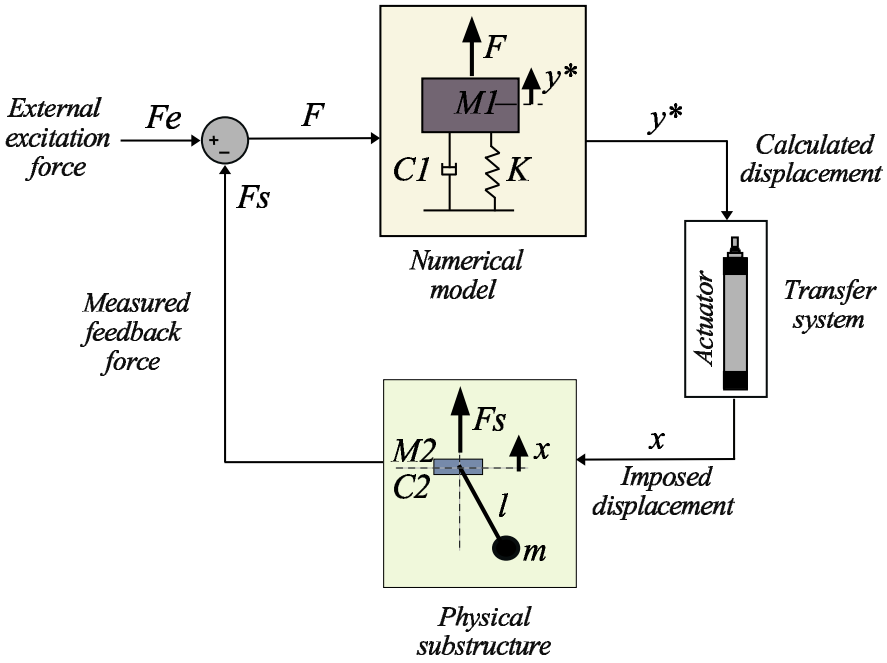

Figure 3.

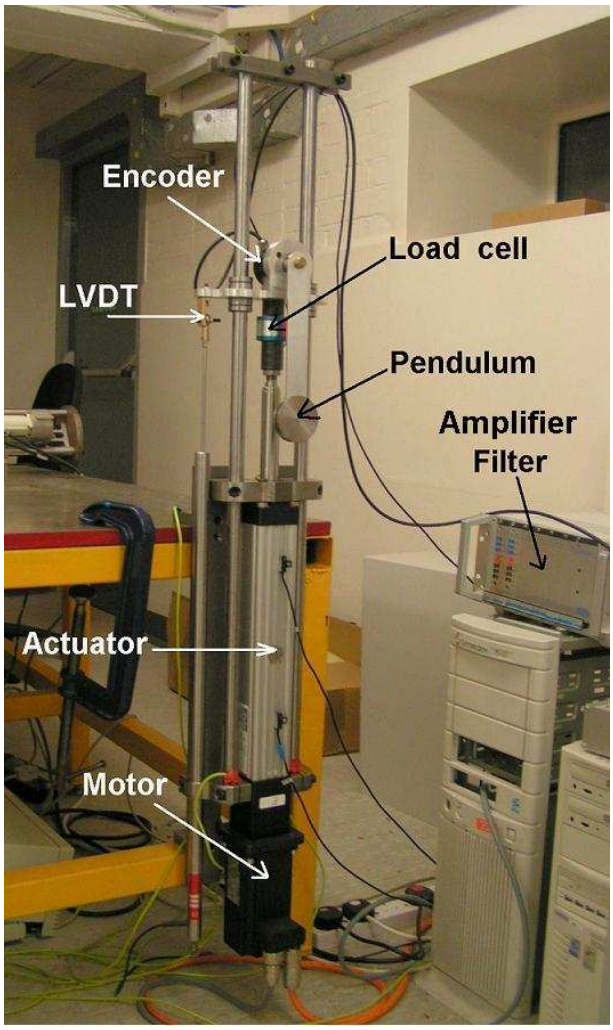

Figure 4.

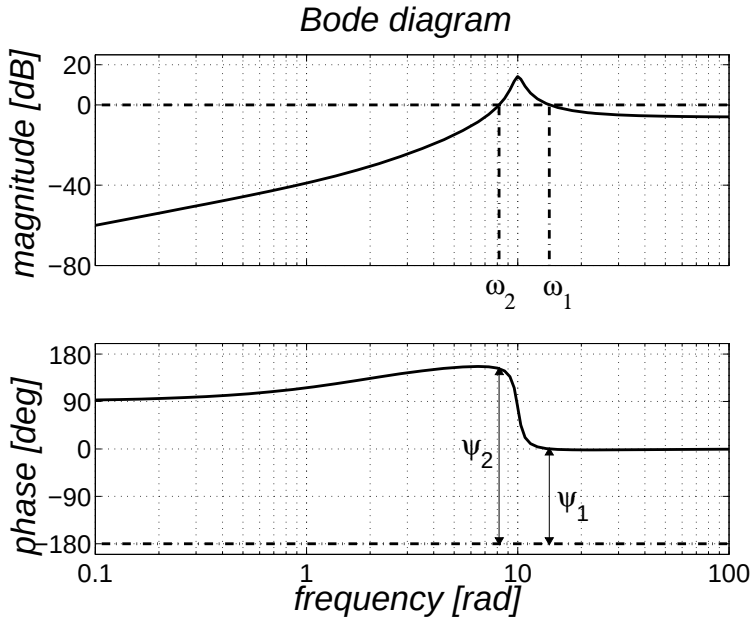

Figure 5.

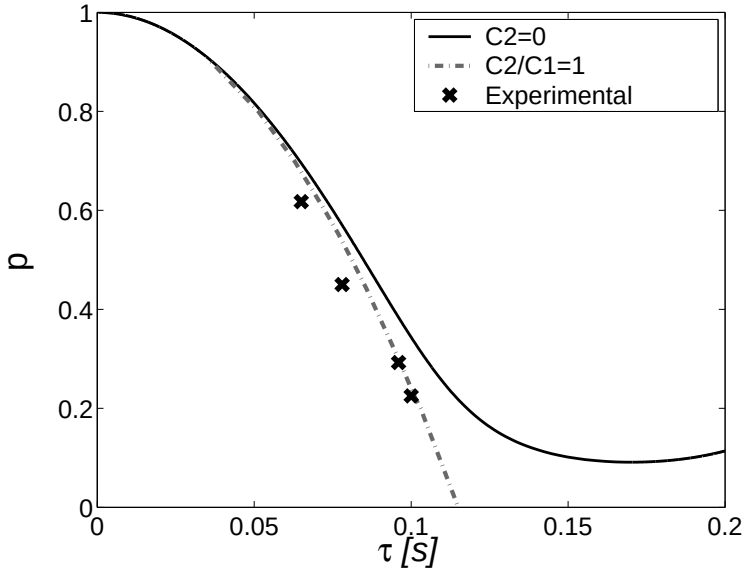

Figure 6.

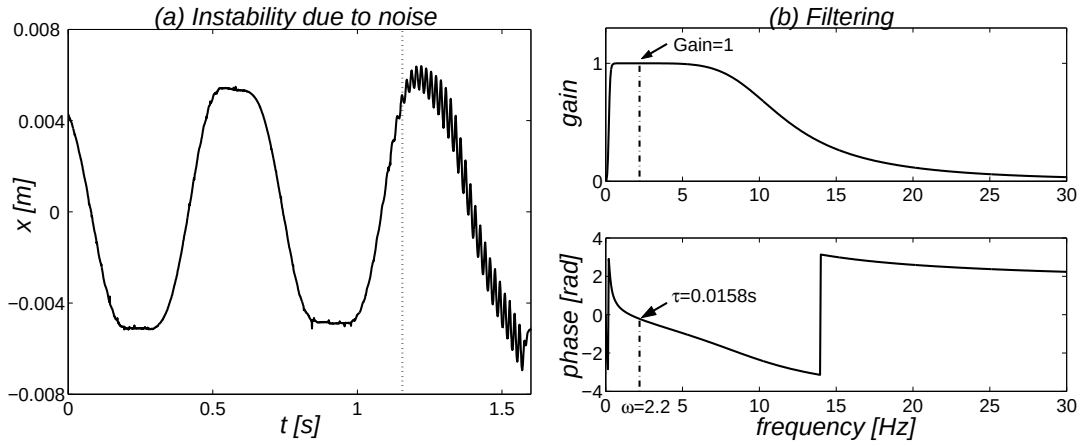

Figure 7.

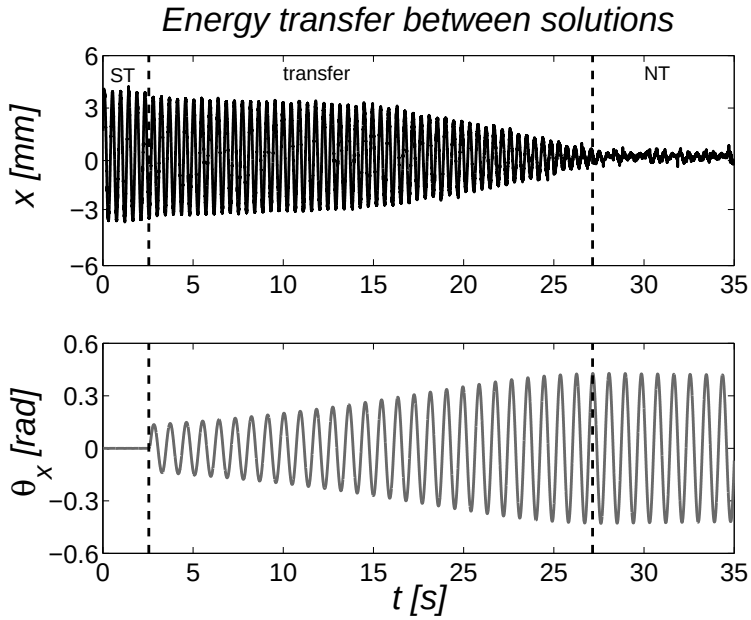

Figure 8.

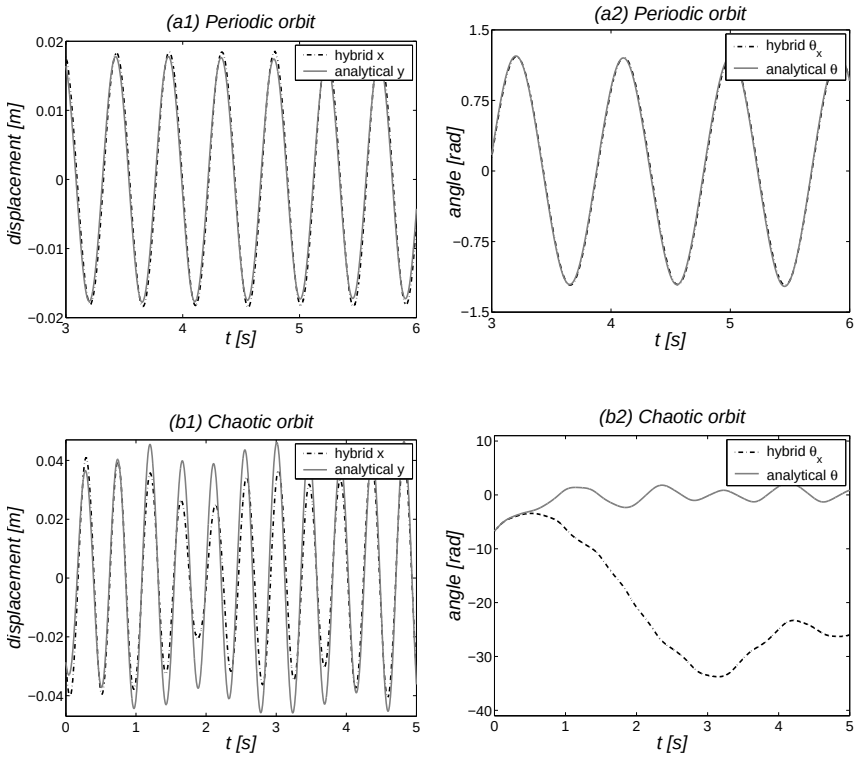

Figure 9.

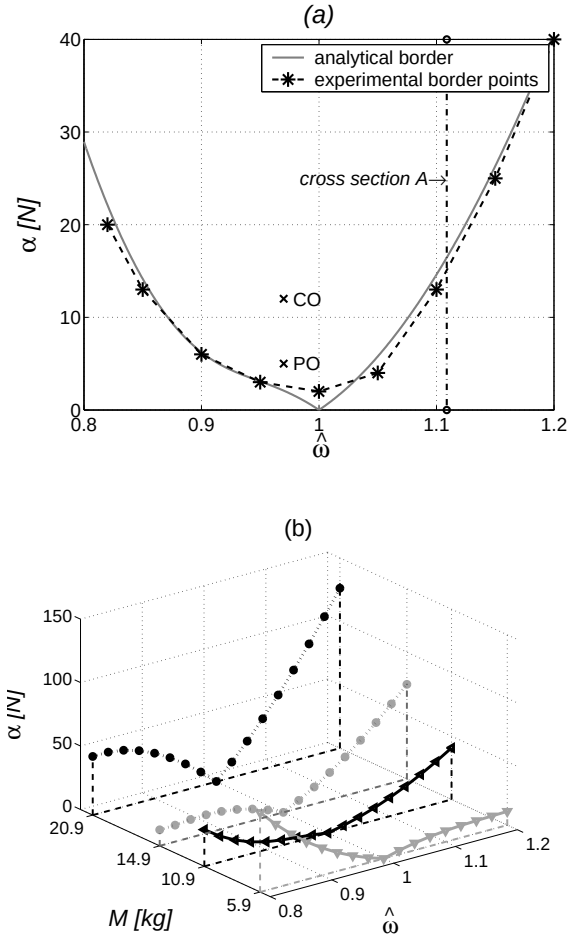

Figure 10.

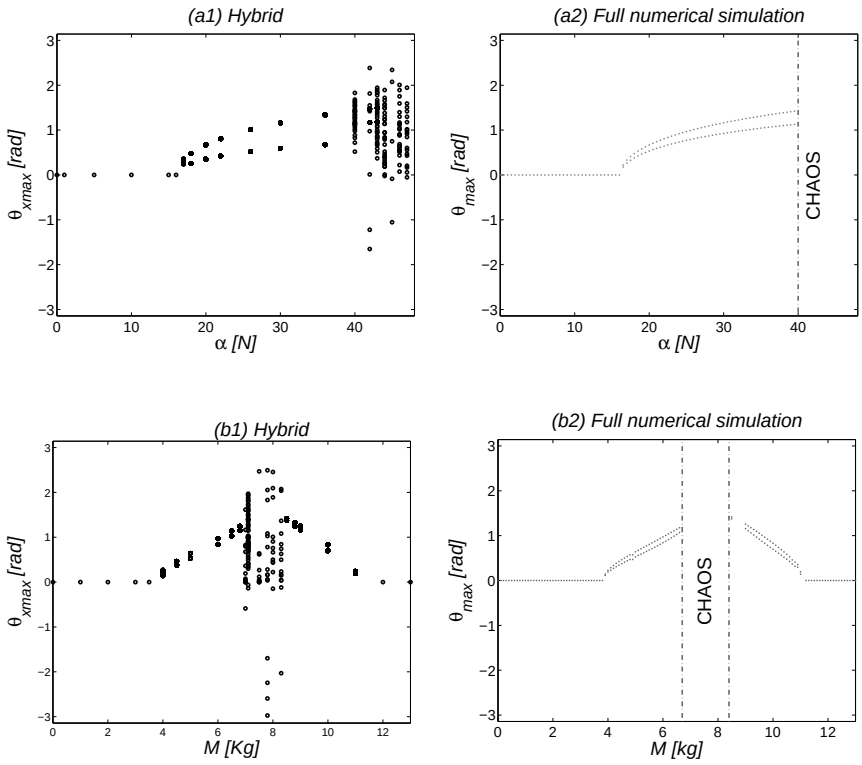

Figure 11.

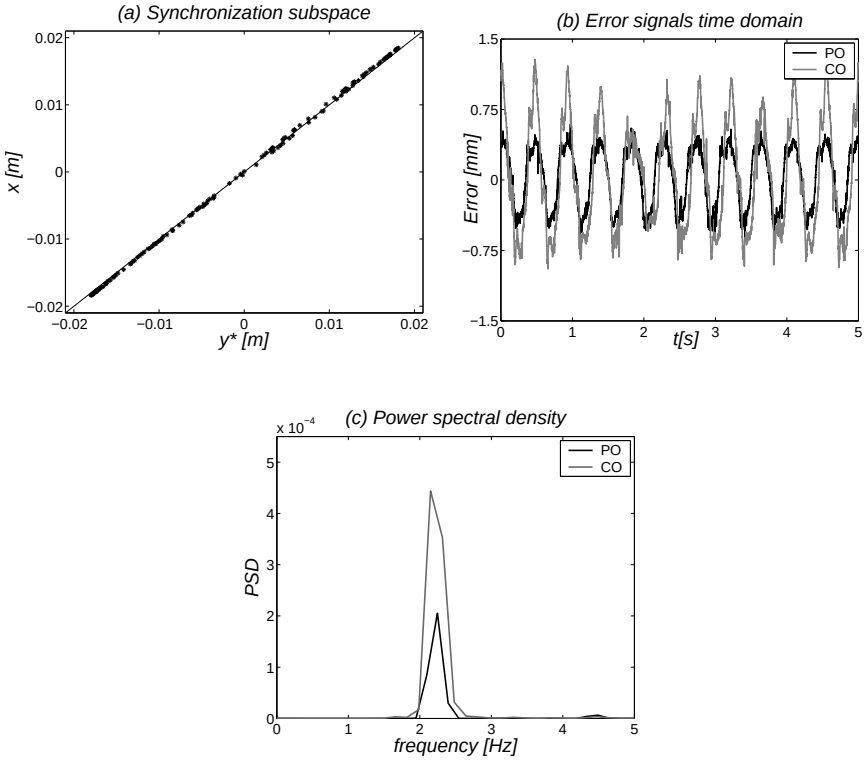

Figure 12.